Open Access

Recent Progress in Materials

LIDSEN Publishing Inc.

Research Article

Phase Equilibrium in ZrO_2-CeO_2-Eu_2O_3 System at a Temperature of 1500 °C

Oksana Kornienko, Anatoliy Sameljuk, Olena Andrievskaya, Serhii Yushkevych, Yurii Bataev

Frantsevich Institute for Materials Science Problems NAS, Kiev - UKRAINE, 3 Krzhizhanovsky str., Kyiv, 03680, Ukraine; E-Mails: kornienkooksana@ukr.net; sam_anatoly@gmx.net; er.andrievskaya@gmail.com; mars970909@gmail.com; yuriibataiev@gmail.com

* **Correspondence:** Oksana Kornienko; E-Mail: kornienkooksana@ukr.net

Academic Editor: Hossein Hosseinkhani

Special Issue: Quantum Mechanics in Solid State Systems

Recent Progress in Materials
2021, volume 3, issue 3
doi:10.21926/rpm.2103036

Received: May 24, 2021
Accepted: August 22, 2021
Published: September 02, 2021

Abstract

The phase equilibria and structural transformations in the ternary ZrO_2-CeO_2-Eu_2O_3 system at 1500 °C were studied by X-ray diffraction and scanning electron microscopy in the overall concentration range. The system was found to constitute fields of solid solutions based on the tetragonal (T) modification of ZrO_2, cubic (C) and monoclinic (B) modifications of Eu_2O_3, cubic with a fluorite-type structure (F) modifications of CeO_2 (ZrO_2), and ordered intermediate phase with a pyrochlore-type structure of $Eu_2Zr_2O_7$ (Py). The refined lattice parameters of the unit cells corresponding to the solid solutions and microstructures of the definite field of compositions for the systems were determined. The peculiarity of the isothermal section of the phase diagram in the ZrO_2-CeO_2-Eu_2O_3 system at 1500 °C is the formation of phase equilibria on the basis of the fluorite solid solutions of ZrO_2(CeO_2) along with other components. There are at least three homogeneous fields of cubic phases. The isothermal section of the ZrO_2-CeO_2-Eu_2O_3 system at 1500 °C was constituted of four three-phase regions (C-Eu_2O_3 + F-CeO_2+Py, C-Eu_2O_3 + F-ZrO_2+Py, Py + F-ZrO_2 + T-ZrO_2, Py + F-CeO_2 + T-ZrO_2).

Keywords
Zirconium and cerium and europium oxides; phase equilibria; solid solutions; functional and structural ceramics

1. Introduction

There are various systems containing oxides of zirconium, cerium, and lanthanides, which are promising alternative materials for the development of heat-protective coatings and fuel cells [1-7]. Environmental pollution is a major concern due to the use of natural carbohydrates and their byproducts in industry and transport. Catalytic neutralization is employed to resolve this problem [8-12]. Generally, the catalysts are composed of noble metals such as Pt, Pd, and Rh. Due to the high cost of precious metals, researchers are seeking new catalytic systems with a high degree of conversion of harmful components. The materials composed of cerium dioxide are promising due to the occurrence of the redox reaction $Ce^{3+} \leftrightarrow Ce^{4+}$ within the system. Due to the nonstoichiometry of cerium dioxide, a large number of oxygen vacancies are formed, which leads to an increase in the mobility of oxygen in the crystal lattice and catalytic activity, as well as the development of oxygen storage capacity (OSC). However, low thermal stability is a significant disadvantage of cerium dioxide. In order to increase thermal stability, it is necessary to introduce zirconium dioxide into the crystal lattice. The doping of $Zr_{1-x}Ce_xO_2$ solid solutions with Ln^{3+} ions increases the formation of defects and, in turn, enhances the catalytic activity of the materials possessing a fluorite-type structure. In addition, the catalytic activity of $M_{0,1}Zr_{0,18}Ce_{0,72}O_2$ in the CO oxidation reaction decreases with the addition of Ln^{3+} species with an increasing atomic number [9]. This is attributed to the occurrence of lanthanide contraction within the system. Also, ZrO_2-CeO_2-Ln_2O_3 systems are widely used for the development of safe and reliable technologies for waste disposal in nuclear industries and the construction of new generation reactors. In addition, materials based on these systems are used as an inert matrix for the immobilization of plutonium. These materials must meet stringent conditions, such as good neutron efficiency, better thermophysical properties, including high thermal conductivity and low thermal expansion, no phase transformations, and stability at high temperatures. In order to fix the transuranic elements, the ceramic matrix is characterized by high thermodynamic stability over time. The ordered pyrochlore phase crystal structure ($A_2B_2O_7$) containing Zr^{4+} as one of the cations in the ideal composition $M_2Zr_2O_7$ (M = three and/or quadrivalent cation) is a highly reliable and reasonable matrix for the retention of multi-concentrated nuclear wastes. It should be noted that $Ln_2Zr_2O_7$ (Py) exists as a disordered fluorite-type phase at high temperatures, while it acquires a pyrochlore-type structure with ordered oxygen vacancies and cations at low temperatures. On the other hand, CeO_2 is widely used as a surrogate material instead of PuO_2 due to their similar physicochemical properties. Therefore, the nodes intended for plutonium ions in the pyrochlore structure will probably be replaced by cerium ions [1-7].

The phase relations in the boundary binary systems ZrO_2-CeO_2 and ZrO_2-Eu_2O_3 were partially studied [13-22], and the phase equilibria data of the CeO_2-Eu_2O_3 system was reportedly contradictory [23-27].

The interaction of zirconium dioxide with cerium dioxide was studied [8-15]. However, there are some differences in the obtained data for phase equilibria at temperatures <1100 °C due to the uncertainty in the eutectoid coordinates of the tetragonal-monoclinic transformation of ZrO_2 and the existence of the $Ce_2Zr_3O_{10}$ (F) phase, and at temperatures >1600 °C due to the possible partial conversion of CeO_2 to Ce_2O_3.

On the low-temperature region (≤1500 ℃) in the state diagram of the ZrO_2-CeO_2 system, the existence of the following phases was revealed: monoclinic M-ZrO_2 in the range of 0 to 1 mol % CeO_2 at 1100 °C, tetragonal T-ZrO_2 from 0 to 18 mol % CeO_2 at 1500 °C and from 2 to 18 mol % CeO_2 at 1100 °C and cubic with a structure of fluorite-type F-CeO_2 in the range of 56 to 100 mol % CeO_2 at 1500 °C and from 73 to 100 mol % CeO_2 at 1100 °C. A wide two-phase region (F+T) in the range of 18-56 mol % CeO_2 was reported at 1500 °C, and two heterogeneous regions were observed at 1100 °C, namely a wide two-phase field (F+T) in the range of 18-73 mol % CeO_2, and a narrow two-phase region (M+T) in the range of 1-2 mol % CeO_2. The tetragonal modification of ZrO_2 does not resist but promotes the formation of the monoclinic phase of M-ZrO_2 [8-10].

The state diagram of the ZrO_2-Eu_2O_3 system has been thoroughly studied in the literature [16, 17]. The liquidus in the ZrO_2-Eu_2O_3 system is characterized by the eutectic transformation of $L_e \leftrightarrows F+X$ (2130 °C, 26 mol % ZrO_2). The solubility limits of Eu_2O_3 in the crystal lattice of T-ZrO_2 are reported to be 1 and 2 mol % at 1250 and 1550 °C, respectively. In addition, the length of the homogeneous region of T+F decreases with temperature from 1-13 mol % Eu_2O_3 at 1250 °C to 2-8 mol % Eu_2O_3 at 1550 °C. The region demonstrating phase homogeneity with a pyrochlore-type structure ($Eu_2Zr_2O_7$) is located in the concentration range of 30-35 and 30-34 mol % at 1250 and 1550 °C, respectively. The cubic structure of pyrochlorine (general formula $A_2B_2O_7$, Fd-3 m) contains large eight coordinated cations A and relatively small octahedral cations B. The pyrochlor has an ordered defective fluorite structure [28]. The structural flexibility in the crystal lattice of pyrochlor allows the partial replacement of A by the B cations, the appearance of oxygen vacancies, and different phases of varying compositions within the structural type. Many compounds are currently known to have a pyrochlor-type structure formed by A^{3+} and B^{4+}, A^{2+} and B^{5+} or combinations of elements, whose average valence corresponds to the A and B cations [29]. Also, the degree of ordering in the structure of pyrochlor depends on its chemical composition [30]. Generally, the pyrochlor structure is preferred for the ratios of the radii of the A and B cations (r_A/r_B) greater than 1.2. In addition, there is a temperature range for the existence of an ordered pyrochlor-type $Ln_2Zr_2O_7$ structure (Ln = La-Ln). For zirconates, the temperature range of this phase decreases from 2280 °C ($La_2Zr_2O_7$) to 1580 °C ($Gd_2Zr_2O_7$) [31]. Above these temperatures, the structure is disordered, resulting in the formation of the fluorite structure. The region of solid solutions possessing a fluorite-type structure undergoes a rupture in the region of an ordered pyrochlore-type structure.

The concentration limits of the solid solutions of F-ZrO_2 are as follows: 13-25 and 37-45 mol % Eu_2O_3 at 1250 °C and 8-28 and 36-52 mol % Eu_2O_3 at 1550 °C.

The dissolution of zirconium dioxide in Eu_2O_3 leads to the stabilization of the C-type cubic phase. The homogeneous region of the solid solutions based on C-Eu_2O_3 are reported to be in the range of 25-15 mol % ZrO_2 at 1250 °C and 21-19 mol % ZrO_2 at 1550 °C. Also, a narrow region of homogeneity is formed in the system on the basis of the monoclinic modification of B-Eu_2O_3 [16, 17].

The binary system CeO_2-Eu_2O_3 was studied in detail [18-22]. In our opinion, the most reliable data on phase equilibria in this system were presented in [22]. There are three types of solid solutions in the CeO_2-Eu_2O_3 system: cubic on the basis of the fluorite F-CeO_2 and C-Eu_2O_3, monoclinic B-Eu_2O_3, and homogeneous regions separated by two-phase fields (F+C) and (C+B), respectively. The

number of phase fields decreases as the temperature reduces to 1000 °C due to the fact that the monoclinic B-modification of Eu_2O_3 exists above 1000 °C. The solubility of Eu_2O_3 in the crystal lattice of F-CeO_2 is reported to be 20 mol % at 1100 and 1500 °C. The length of the homogeneous region of the solid solution based on B-Eu_2O_3 is <1 mol %.

There have been no studies on the phase equilibria of the ZrO_2-CeO_2-Eu_2O_3 system in the literature. Meanwhile, the phase equilibria of the ternary systems of the ZrO_2-CeO_2-Ln_2O_3 (Ln = La, Gd, Dy, Y, Yb) series have been extensively studied [32-38]. In these ternary systems, thesolid solutions depends on various polymorphic modifications of the initial components, as well as the existence of phases with a pyrochlor-type $Ln_2Zr_2O_7$ (Pr) structure and $Zr_3Ln_4O_{12}$ (δ) phases. It should be noted that the formation of an ordered phase with a pyrochlor-type structure is a characteristic feature of cerium subgroup systems. The homogeneous region of the ordered pyrochlor-type structured phase narrows with the decreasing ionic radius of the lanthanide. Meanwhile, the existence of the δ-phase has been established to be unique for the ternary ZrO_2-CeO_2-Ln_2O_3 (Ln = Y, Yb) systems [32, 38].

2. Experimental

Zirconium oxide nitrate $ZrO(NO_3)_2 \cdot H_2O$, cerium oxide nitrate $Ce(NO_3)_3 \cdot 6H_2O$, europium oxide Eu_2O_3 (all 99.99%), and analytical-grade nitric acid were used as the starting materials for the ZrO_2-CeO_2-Eu_2O_3 system. The oxides were dried in a muffle chamber at 1200 °C (2 h) before weighing them out.%. The weighed oxide portions were dissolved in HNO_3 (1:1), evaporated, and calcined at 800 °C for 2 h. The powders were subjected to single-action pressing in a steel die without a binder at 10-30 MPa to make pellets with the dimensions of 5 mm diameter and 4 mm height. The obtained samples for the study of the phase equilibria of the ternary ZrO_2-CeO_2-Eu_2O_3 system at 1500 °C were subjected to a two-stage heat treatment: 1) calcination in a laboratory muffle furnace (*SNOL 10/1300 LHM01*) with heaters H23U5T (fehral) at 1100 °C for 452 h to remove nitrate residues, and 2) annealing in a high-temperature furnace (*Micropyretics Heaters International M18-40*) with molybdenum disilicide heaters ($MoSi_2$) at 1500 °C for 150 h in air, resulting in the diffusion-controlled leveling of the composition in accordance with the state diagram of the system. The completion of the synthesis was regularly monitored. Furthermore, the samples were pressed and annealed again. Upon annealing for 150 h (1500 °C), there was no change in the phase composition of the samples. The samples were cooled inside the furnace.

After heat treatment, the obtained samples were ground in an agate mortar to form a homogeneous powder. The resultant powder was taken in a cuvette, which was screwed to the holder upon the installation of DRON-3. Using the DRON-3 diffractometer (Joint Stock Company "Bourevestnik"), the X-ray diffraction (XRD) pattern was obtained at room temperature (CuK- radiation, Ni-filter) to analyze the phases. The modes used in the study were as follows: scanning step was 0.05-0.1 deg, exposure was set as 4 s, and 2θ angles were in the range of 10 to 100°. The experimental result is dependent on the intensity of the diffracted radiation on the angle of reflection. The International Powder Standards Committee database (JSPSDS International Center for Diffraction Data 1999) was used to identify the obtained X-ray diffraction patterns.

The refractive indices were measured in highly refractive immersion media (sulfur-selenium alloys or solutions of arsenic tri-bromide in methylene iodide) with an accuracy of ±0.02.

The samples for the microstructural studies were prepared using a Buehler grinding and polishing machine. The microstructures were studied using the scanning electron microscope SUPERPROBE-733

(*"JEOL, Japan, Palo Alto, CA*) with the help of back-reflected electrons (BSE) on the undigested sections of the annealed samples with a gold-plated sample.

3. Results and Discussion

The formation of new phases in the ZrO_2-CeO_2-Eu_2O_3 system was not established at 1500 °C. At 1500 °C, solid solution fields were formed on the basis of tetragonal (T) and cubic (F) phases with fluorite structured modifications of ZrO_2, monoclinic (B) and cubic (C) modifications of Eu_2O_3, cubic modification of CeO_2 with a fluorite (F) structure and ordered phase with a pyrochlore $Eu_2Zr_2O_7$ (Py) structure.

Based on the obtained results, an isothermal cross-section of the state diagram of the ZrO_2-CeO_2-Eu_2O_3 system was constructed at 1500 °C (Figure 1). The original chemical and phase compositions of the samples at 1500 °C, and the parameters of the unit cells of the phases in equilibrium at a given temperature are shown in Table 1.

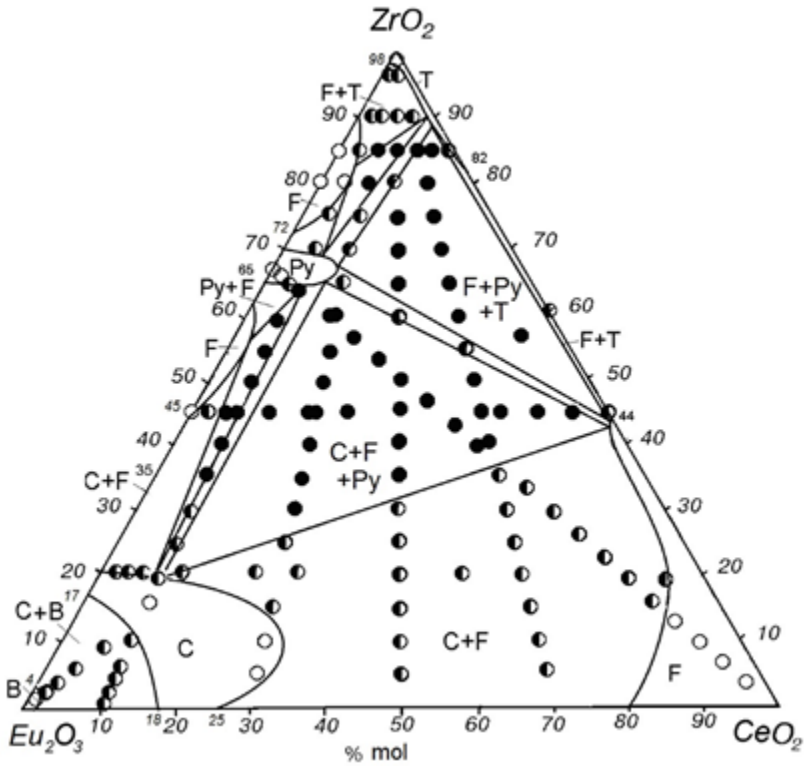

Figure 1 Isothermal section of the ZrO_2-CeO_2-Eu_2O_3 system at 1500 °C, ○ -single-phase samples; ◐-two-phase samples; ●-three-phase samples.

Table 1 Chemical and phase compositions, and lattice parameters of the phases in the ZrO_2-CeO_2-Eu_2O_3 system after annealing at 1500 °C for 150 h. (XRD, petrography and microscopy data).

Chemical composition, mol %			Phase compositions and parameters of elementary cells, nm
ZrO_2	CeO_2	Eu_2O_3	
Section ZrO_2-(50 mol % CeO_2-50 mol % Eu_2O_3)			

5	47.5	47.5	<F-CeO_2> (a = 0.5432) + <C-Eu_2O_3> (a = 1.0864)
10	45	45	<F-CeO_2> (a = 0.5397) + <C-Eu_2O_3> (a = 1.0794)
15	42.5	42.5	<F-CeO_2> (a = 0.5409) + <C-Eu_2O_3> (a = 1.0827)
20	40	40	<F-CeO_2> (a = 0.5392) + <C-Eu_2O_3> (a = 1.0807)
25	37.5	37.5	<F-CeO_2> (a = 0.5411) + <C-Eu_2O_3> (a = 1.0827)
30	35	35	<F-CeO_2> (a = 0.5370) + <C-Eu_2O_3> (a = 1.0743)
35	32.5	32.5	<F-CeO_2> (a = 0.5350) + <C-Eu_2O_3> (a = 1.0805) + Py
40	30	30	<F-CeO_2> + <C-Eu_2O_3> (a = 1.0894) + Py
45	27.5	27.5	<F-CeO_2> + <C-Eu_2O_3> + Py
50	25	25	<F-CeO_2> + <C-Eu_2O_3> + Py
55	22.5	22.5	<F-CeO_2> + Py + <C-Eu_2O_3>
60	20	20	<F-CeO_2> + Py
65	17.5	17.5	<F-ZrO_2> + Py + <T-ZrO_2>*
70	15	15	<F-ZrO_2> +Py + <T-ZrO_2>*
75	12.5	12.5	<F-ZrO_2> +Py + <T-ZrO_2>*
80	10	10	Py + <T-ZrO_2>*↑
85	7.5	7.5	<F-ZrO_2> + <T-ZrO_2>* + Py
90	5	5	<F-ZrO_2> + <T-ZrO_2>*
95	2.5	2.5	<F-ZrO_2> + <T-ZrO_2>*
96	2	2	<F-ZrO_2> + <T-ZrO_2>*
97	1.5	1.5	<T-ZrO_2>* + <F-ZrO_2>
98	1	1	<T-ZrO_2>* + <F-ZrO_2>
99	0.5	0.5	<T-ZrO_2>*
Section CeO_2-(67 mol % ZrO_2 - 33 mol % Eu_2O_3)			
66	1	33	Py ($Eu_2Zr_2O_7$)
65	2	33	Py + <F-ZrO_2>
64	3	33	Py + <F-ZrO_2>
64	4	32	Py + <F-ZrO_2>
63	5	32	<F-CeO_2> (a = 0.5315) + Py + <C-Eu_2O_3
60	10	30	<F-CeO_2> (a = 0.5320) + Py + <C-Eu_2O_3
57	15	28	<F-CeO_2> (a = 0.5319) + Py + <C-Eu_2O_3
53	20	27	<F-CeO_2> (a = 0.5317) + Py + <C-Eu_2O_3>
47	30	23	<F-CeO_2> (a = 0.5318) + Py + <C-Eu_2O_3>
44	35	21	<F-CeO_2> (a = 0.5319) + Py + <C-Eu_2O_3>
40	40	20	<F-CeO_2> (a = 0.5318) + Py + <C-Eu_2O_3>
37	45	18	<F-CeO_2> (a = 0.5319) + Py + <C-Eu_2O_3>
34	50	16	<F-CeO_2> (a = 0.5322) + <C-Eu_2O_3>
30	55	15	<F-CeO_2> (a = 0.5336) + <C-Eu_2O_3>
26	60	14	<F-CeO_2> (a = 0.5356) + <C-Eu_2O_3>
23	65	12	<F-CeO_2> (a = 0.5368) + <C-Eu_2O_3>
20	70	10	<F-CeO_2> (a = 0.5369) + <C-Eu_2O_3>
17	75	8	<F-CeO_2> (a = 0.5374) + <C-Eu_2O_3>

13.5	80	6.5	<F-CeO_2> (a = 0.5381)
10	85	5	<F-CeO_2> (a = 0.5386)
7	90	3	<F-CeO_2> (a = 0.5390)
3	95	2	<F-CeO_2> (a = 0.5397)
Section ZrO_2-(30 mol % CeO_2-70 mol % Eu_2O_3)			
5	29	66	<C-Eu_2O_3> (a = 1.0849)
10	27	63	<C-Eu_2O_3> (a = 1.0819)
15	25.5	59.5	<C-Eu_2O_3> (a = 1.0802) + <F-CeO_2>
25	22	53	<C-Eu_2O_3> (a = 1.0737) + <F-CeO_2>
30	21	49	<C-Eu_2O_3> (a = 1.0738) + <F-CeO_2> + Py
40	18	42	<C-Eu_2O_3> (a = 1.0672) + <F-CeO_2>+ Py
45	16.5	38.5	<C-Eu_2O_3> (a = 1.0657) + <F-CeO_2> + Py
50	15	35	<C-Eu_2O_3> (a = 1.0621) + <F-CeO_2> + Py
55	13.5	31.5	<C-Eu_2O_3> (a = 1.0580) + <F-CeO_2> + Py
65	10	25	<F-CeO_2> + Py
70	9	21	Py + <T-ZrO_2>
75	8.5	16.5	Py + <T-ZrO_2>
80	6	14	<F-ZrO_2> + Py + <T-ZrO_2>
85	5.5	9.5	<F-ZrO_2> + <T-ZrO_2>* + Py
90	3	7	<F-ZrO_2> + <T-ZrO_2>*
Section ZrO_2-(70 mol % CeO_2-30 mol % Eu_2O_3)			
5	66	29	<F-CeO_2> + <C-Eu_2O_3>
10	63	27	<F-CeO_2> + <C-Eu_2O_3>
15	59.5	25.5	<F-CeO_2> + <C-Eu_2O_3>
25	53	22	<F-CeO_2> + <C-Eu_2O_3>
30	49	21	<F-CeO_2> + <C-Eu_2O_3> сл.
40	42	18	<F-CeO_2> + <C-Eu_2O_3> + Py
45	38.5	16.5	Py + <F-CeO_2> + <C-Eu_2O_3>
50	35	15	Py + <F-CeO_2> + <C-Eu_2O_3>
55	31.5	13.5	Py осн.+ <F-CeO_2>
65	25	10	Py + <F-CeO_2> + <T-ZrO_2>*
70	21	9	Py + <F-CeO_2> + <T-ZrO_2>*
75	16.5	8.5	Py + <F-CeO_2> + <T-ZrO_2>*
80	14	6	Py + <F-CeO_2> + <T-ZrO_2>*
85	9.5	5.5	<F-CeO_2> + <T-ZrO_2>* + Py
90	7	3	<F-ZrO_2> + <T-ZrO_2>*
Section ZrO_2-(10 mol % CeO_2-90 mol % Eu_2O_3)			
2	10	88	<C-Eu_2O_3> (a = 1.0847) + <B-Eu_2O_3>
3	10	87	<C-Eu_2O_3> осн. (a = 1.0844) + <B-Eu_2O_3>
4	9.5	86.5	<C-Eu_2O_3> (a = 1.0837) + <B-Eu_2O_3>
5	9.5	85.5	<C-Eu_2O_3> (a = 1.0829) + <B-Eu_2O_3>
10	9.5	80.5	<C-Eu_2O_3> (a = 1.0821) + <B-Eu_2O_3>

15	9	76	<C-Eu_2O_3> (*a* = 1.0810)
20	8	72	<C-Eu_2O_3> (*a* = 1.0803) + Py
25	8	67	<C-Eu_2O_3> (*a* = 1.0786) + Py
30	8	62	<C-Eu_2O_3> (*a* = 1.0763) + Py↑
35	8	57	<C-Eu_2O_3> (*a* = 1.0750) + <F-ZrO_2> + Py
40	7	53	<C-Eu_2O_3>(*a* = 1.0748) + <F-ZrO_2> + Py
45	6.5	48.5	<C-Eu_2O_3> (*a* = 1.0751) + <F-ZrO_2> + Py
50	6	44	<C-Eu_2O_3> (*a* = 1.0753) + <F-ZrO_2> + Py
55	5.5	39.5	<C-Eu_2O_3> (*a* = 1.0749) + <F-ZrO_2> + Py
60	5	35	<C-Eu_2O_3>(*a* = 1.0750) + <F-ZrO_2> + Py
70	4	26	<F-ZrO_2> + Py
75	3	22	<F-ZrO_2> + Py
80	2.5	17.5	<F-ZrO_2>
85	1.5	13.5	<F-ZrO_2> + <T-ZrO_2>*
90	1.5	8.5	<T-ZrO_2>* + <F-ZrO_2>
Section Eu_2O_3-(60 mol % ZrO_2-40 mol % CeO_2)			
60	40	0	<T-ZrO_2>** + <F-CeO_2>
57	38	5	<F-CeO_2> + Py + <T-ZrO_2>
53.5	36.5	10	<F-CeO_2> + Py
39.5	25.5	35	<F-CeO_2> + <C-Eu_2O_3> + Py
36	24	40	<F-CeO_2> + <C-Eu_2O_3> + Py
9.5	5.5	85	<B-Eu_2O_3> + <C-Eu_2O_3>
6	4	90	<B-Eu_2O_3> + <C-Eu_2O_3>
3	2	95	<B-Eu_2O_3> + <C-Eu_2O_3>
2.5	1.5	96	<B-Eu_2O_3> + <C-Eu_2O_3>
2	1	97	<B-Eu_2O_3> + <C-Eu_2O_3>
1.5	0.5	98	<B-Eu_2O_3> + <C-Eu_2O_3>
0.5	0.5	99	<B-Eu_2O_3> + <C-Eu_2O_3>
Iso-concentration line 20 mol % ZrO_2			
20	1	79	<C-Eu_2O_3> + <F-ZrO_2>
20	2	78	<C-Eu_2O_3> + <F-ZrO_2>
20	3	77	<C-Eu_2O_3> + <F-ZrO_2>
20	4	76	<C-Eu_2O_3> + <F-ZrO_2>
20	10	70	<C-Eu_2O_3> + <F-CeO_2>
20	20	60	<C-Eu_2O_3> + <F-CeO_2>
20	25	55	<C-Eu_2O_3> + <F-CeO_2>
20	30	50	<C-Eu_2O_3> + <F-CeO_2>
20	35	45	<C-Eu_2O_3> + <F-CeO_2>
20	45	35	<C-Eu_2O_3> + <F-CeO_2>
20	55	25	<C-Eu_2O_3> + <F-CeO_2>
20	65	15	<C-Eu_2O_3> + <F-CeO_2>
20	75	5	<C-Eu_2O_3> + <F-CeO_2>

20	80	0	<F-CeO_2>
Iso-concentration line 45 mol % ZrO_2			
45	2	53	<F-ZrO_2> + <C-Eu_2O_3>
45	3	62	<F-ZrO_2> + <C-Eu_2O_3>
45	4	51	<F-ZrO_2> + <C-Eu_2O_3>
45	5	50	<F-ZrO_2> + <C-Eu_2O_3> + Py
45	20	35	<F-CeO_2> + <C-Eu_2O_3> + Py
45	45	10	<F-CeO_2> + <C-Eu_2O_3> + Py
45	50	5	<F-CeO_2> + <C-Eu_2O_3> + Py
45	55	0	<F-ZrO_2> + <T-ZrO_2>*
Iso-concentration line 85 mol % ZrO_2			
85	0	15	<F-ZrO_2>
85	11	4	<F-CeO_2> + <T-ZrO_2>* + Py
85	12	3	<F-CeO_2> + <T-ZrO_2>* + Py
85	13	2	<F-CeO_2> + <T-ZrO_2>**↑ + Py
85	14	1	<F-CeO_2> + <T-ZrO_2>**
85	15	0	<T-ZrO_2>**

* Under given conditions (T= 1500 °C, 150 h, in air, slow cooling), the tetragonal phase T-ZrO_2 is not stable, while the monoclinic phase M-ZrO_2 is stable;

** The partial stabilization of T-ZrO_2 was observed.

In order to determine the boundaries of the phase fields, the concentration dependencies of the parameters of the unit cells of the formed phases were used along with the phase composition data of the samples (Figures 2-4).

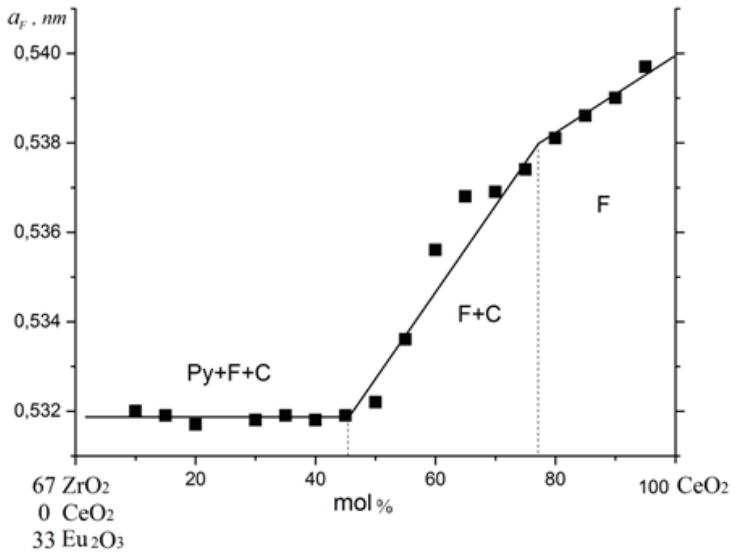

Figure 2 Concentration dependencies of the lattice parameters of the solid solutions based on the F-CeO_2 in the CeO_2-(67 mol % ZrO_2-33 mol % Eu_2O_3) section of the ZrO_2-CeO_2-Eu_2O_3 system after annealing the samples at 1500 °C.

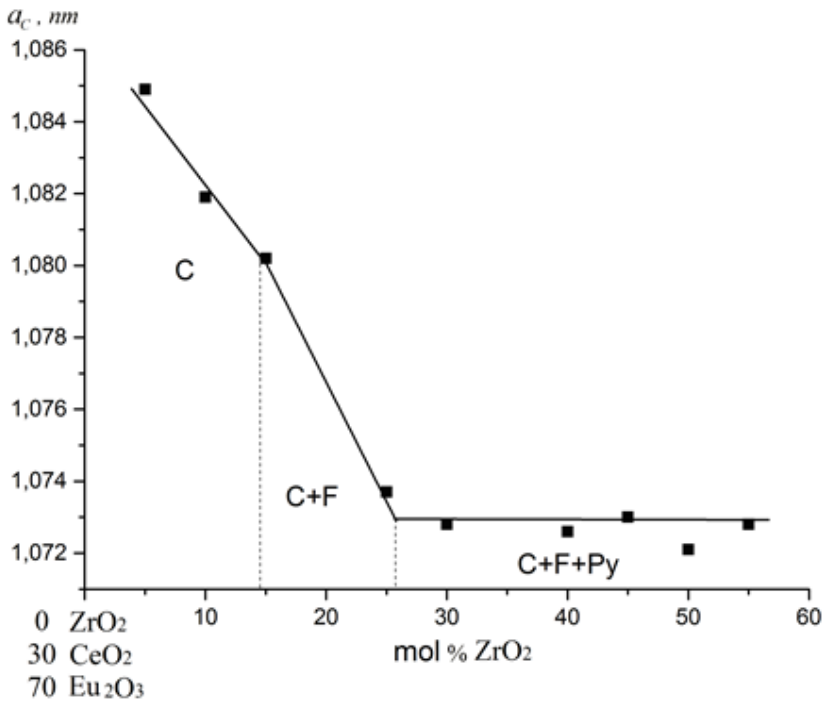

Figure 3 Concentration dependencies of the lattice parameters of the solid solutions based on the C-Eu_2O_3 in the ZrO_2-(30 mol % CeO_2-70 mol % Eu_2O_3) section of the ZrO_2-CeO_2-Eu_2O_3 system after annealing the samples at 1500 °C.

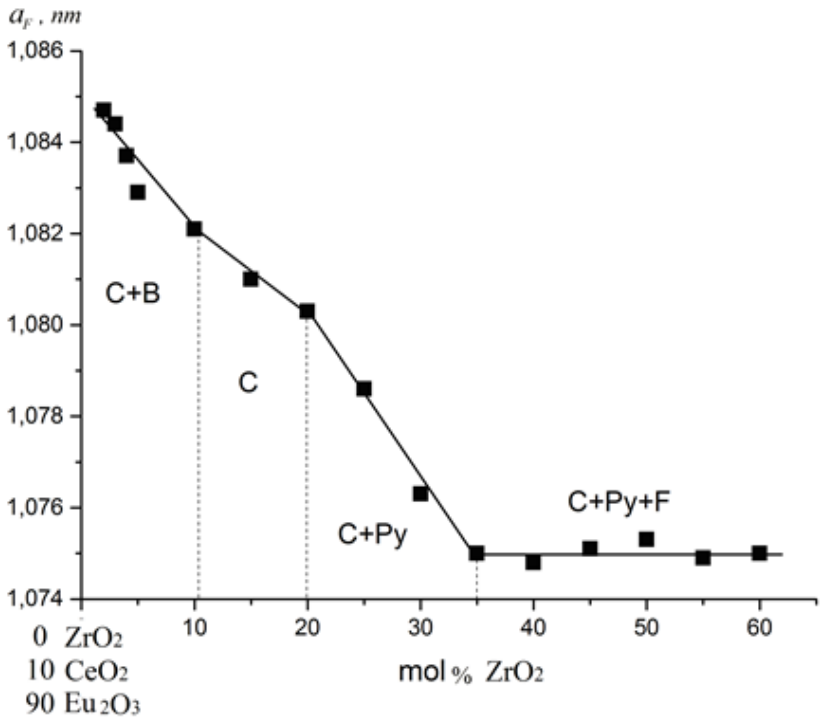

Figure 4 Concentration dependencies of the lattice parameters of solid solutions based on the C-Eu_2O_3 in the ZrO_2-(10 mol % CeO_2-90 mol % Eu_2O_3) section of the ZrO_2-CeO_2-Eu_2O_3 system after annealing the samples at 1500 °C.

Based on the parameters of the unit cell of the Py phase in the three-phase regions, X-ray diffraction data and electron microscopy results, the coordinates of the figurative points of the Py phase on the vertices of the triangles of the three-phase regions (Py+T+F-CeO_2), (Py+T+F-ZrO_2), (Py+C+F-ZrO_2) and (Py+C+F-CeO_2), are shown in Table 2.

Table 2 Coordinates of the tie-line triangles in the ZrO_2-CeO_2-Eu_2O_3 system after annealing the samples at 1500 °C.

Phase	Coordinates of the tie-line triangles, mol %									
Field	T		Py		F-CeO_2		F-ZrO_2		C	
	ZrO_2	CeO_2	ZrO_2	CeO_2	ZrO_2	CeO_2	ZrO_2	CeO_2	ZrO_2	CeO_2
Py+T+F-CeO_2	88	10	67	7	43	56	-	-	-	-
Py+T+F-ZrO_2	90	8	68	5	-	-	83	3	-	-
Py+C+F-ZrO_2	-	-	65	5	-	-	57	2	19	6
Py+C+F-CeO_2	-	-	66	10	42	56	-	-	19	8

The characteristic microstructures of the samples located in different phase fields on the state diagram of the ZrO_2-CeO_2-Eu_2O_3 system at 1500 °C are presented in Figure 5.

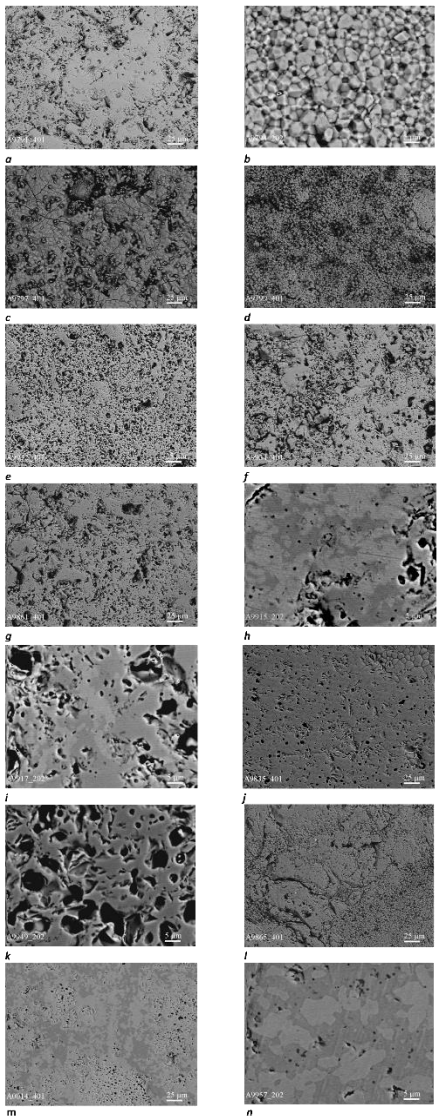

Figure 5 Microstructure of ZrO_2-CeO_2-Eu_2O_3 samples after annealing at 1500 °C (***a***-99 mol % ZrO_2-0.5 mol % CeO_2-0.5 mol % Eu_2O_3, <T-ZrO_2>*; ***b***-66 mol % ZrO_2-1 mol % CeO_2-33 mol % Eu_2O_3, Py ($Eu_2Zr_2O_7$), BEI, × 2000; ***c***-64 mol % ZrO_2-3 mol % CeO_2-33 mol % Eu_2O_3, Py + <F-ZrO_2>, BEI, × 400; ***d***-64 mol % ZrO_2-4 mol % CeO_2-32 mol % Eu_2O_3, Py + <F-ZrO_2>, BEI, × 400; ***e***-70 mol % ZrO_2-4 mol % CeO_2-26 mol % Eu_2O_3, <F-ZrO_2> + Py, BEI, × 400; ***f***-75 mol % ZrO_2-3 mol % CeO_2-22 mol % Eu_2O_3, <F-ZrO_2> + Py, BEI, × 400; grey phase - Py, dark phase-<F-ZrO_2>, black - pores; ***g***-75 mol % ZrO_2-8.5 mol % CeO_2-16.5 mol % Eu_2O_3, Py осн. + <T-ZrO_2>, BEI, × 400; ***h***-25 mol % ZrO_2-8.5 mol % CeO_2-66.5 mol % Eu_2O_3, <C-Eu_2O_3> + Py, BEI, × 2000; grey phase - Py, dark phase-<F-ZrO_2>, black - pores; ***i***-30 mol % ZrO_2-8 mol % CeO_2-62 mol % Eu_2O_3, <C-Eu_2O_3> + Py↑, BEI, × 2000; ***j***-3 mol % ZrO_2-95 mol % CeO_2-2 mol % Eu_2O_3, <F-CeO_2>, BEI, × 400; ***k***-53.5 mol % ZrO_2-36.5 mol % CeO_2-10 mol % Eu_2O_3, <F-CeO_2> + Py, BEI, × 2000; ***l***-80 mol % ZrO_2-6 mol % CeO_2-14 mol % Eu_2O_3, <F-ZrO_2> + Py + <T-ZrO_2>, BEI, × 2000; grey phase-<F-CeO_2>, grey porous phase-$Eu_2Zr_2O_7$; ***m***-85 mol % ZrO_2-11 mol % CeO_2-4 mol % Eu_2O_3, <F-CeO_2> + <T-ZrO_2>* + Py, BEI, × 400; light porous phase-<F-CeO_2>, light grey porous phase- $E_2Zr_2O_7$ (Py), dark phase-<T-ZrO_2>*, blake - pores; ***n***-6 mol % ZrO_2-4 mol % CeO_2-90 mol % Eu_2O_3, <B-Eu_2O_3> + <C-Eu_2O_3>, BEI, × 2000.)

At 1500 °C, seven regions of the solid solutions based on the T-and F-modifications of ZrO_2, F-CeO_2, C-and B-Eu_2O_3, as well as intermediate phase of europium zirconate $Eu_2Zr_2O_7$ (Py) were observed.

On the regions with a high concentration of ZrO_2, solid solutions are formed on the basis of the tetragonal modification of ZrO_2. The solubility of Eu_2O_3 in T-ZrO_2 was as low as ~1 mol. %, as confirmed by the X-ray diffraction data. The boundary of the homogeneous region of the solid solution based on T-ZrO_2 at 1500 °C passed through the compositions: 98 mol % ZrO_2-1 mol % CeO_2-1 mol % Eu_2O_3, 90 mol % ZrO_2-7 mol % CeO_2-3 mol % Eu_2O_3, 85 mol % ZrO_2-14 mol % CeO_2-1 mol % Eu_2O_3-two-phase (T+F), 85 mol % ZrO_2-9.5 mol % CeO_2-5.5 mol % Eu_2O_3-three-phase (T+F+Py).

In the ternary system, the oxides of cerium and europium dissolved upon the tetragonal modification of zirconium dioxide in the same amount as observed in the binary systems of ZrO_2-Eu_2O_3 and ZrO_2-CeO_2. The solid solutions based on the T-modification of ZrO_2 do not harden on employing the cooling modes. The X-ray diffractions of the samples obtained at room temperature showed the characteristic lines of M-ZrO_2. A fully stabilized tetragonal modification of T-ZrO_2 was observed in the two-phase and three-phase samples with a cross-section of ZrO_2-(70 mol % CeO_2-30 mol % Eu_2O_3) in formulations containing 70 mol % ZrO_2-9 mol % CeO_2-21 mol % Eu_2O_3, 75 mol % ZrO_2-8.5 mol % CeO_2-16.5 mol % Eu_2O_3, 80 mol % ZrO_2-6 mol % CeO_2-14 mol % Eu_2O_3. The petrographic studies revealed traces of the phase transitions manifested in the form of polysynthetic twinning. The microstructure of the solid solution based on the T* modification of ZrO_2 is presented in Figure 5 a.

The solid solution formed by europium zirconate at 1500 °C was in equilibrium with all the phases existing in the ZrO_2-CeO_2-Eu_2O_3 system, except for the monoclinic B-modification of europium oxide, resulting in the formation of solid substitution solutions with the phases of the binary systems. The phase-based field of the solid solutions with a pyrochlore (Py)-type structure was directed in the direction of the ZrO_2-CeO_2 limiting system. The highest solubility of cerium dioxide in $Eu_2Zr_2O_7$ reached 7 mol % CeO_2 (Table 1) along the beam of 67 mol % ZrO_2, attributing to the intermediate size of the Ce^{4+} ion (r = 0.090 nm) among the Eu^{3+} (r = 0.0985 nm) and Zr^{4+} (r = 0.079 nm) ions. The microstructure of the phase-based solid solution with a pyrochlore-type structure possessing different grain orientations is shown in 4.5.b. The microstructure of the single-phase sample of 66 mL % ZrO_2-1 mol % CeO_2-33 mol % Eu_2O_3 is represented by large and small (0.8-10.8 μm) polyhedral grains (Figure 5 b).

The micro-X-ray spectral analysis showed that the sample possessed a single phase, where all the elements (Zr, Eu) were distributed uniformly over the investigated surface. This is consistent with the X-ray diffraction data suggesting the formation of a solid solution based on the ordered $Eu_2Zr_2O_7$ (Py) phase (Table 1). The microstructures of the samples in the two-phase region (Py+F-ZrO_2) are presented in Figure 5 c-d. The samples with 65 mol % ZrO_2-2 mol % CeO_2-33 mol % Eu_2O_3 and 64 mol % ZrO_2-3 mol % CeO_2-33 mol % Eu_2O_3 revealed two distinct structural components (Figure 5 c-d). Based on the results of the micro-X-ray spectral analysis, the dark phase was composed of zirconium alone and thus possessed the F-ZrO_2 phase, while the grey phase was enriched with europium and zirconium and thus identified as the $Eu_2Zr_2O_7$ (Py) phase, as confirmed by the X-ray diffraction and petrography. With the increase in the ZrO_2 concentration, the number of pyrochlore-type phases increased, resulting in a change in the morphology of the samples. Based on the petrography results of the above compositions, two isotropic phases were observed, namely the basis isotropic phase (Py), and the second (F) phase observed in much smaller quantities. The cross-

section of CeO_2-(67 mol % ZrO_2-33 mol % Eu_2O_3) in the samples containing 2-4 mol % CeO_2 clearly revealed a two-phase fine-grained structure, with an isotropic pyrochlore-structured phase, as well as an isotropic fluorite-structured phase in much smaller quantities. The microstructures of the two-phase samples (Py+F-ZrO_2) with the compositions of 70 mol % ZrO_2-4 mol % CeO_2-26 mol % Eu_2O_3 and 75 mol % ZrO_2-3 mol % CeO_2-22 mol % Eu_2O_3 in the cross-section of ZrO_2-(10 mol % CeO_2-90 mol % Eu_2O_3) differs markedly in its morphology (Figure 5 e, f). The structures of these samples were manifested in the form of perforated and smooth grey areas on the surfaces, where the grey smooth area corresponded to the <F-ZrO_2> phase, and the grey porous phase showed a perforated $Eu_2Zr_2O_7$ (Py) structure.

The characteristic microstructure of the two-phase region (Py+T) is presented in Figure 4.5 j. Both the phases were clearly manifested in their morphology. Based on the qualitative micro-X-ray spectral analysis, the smooth grey phase was enriched with zirconium and, apparently, corresponded to a solid solution based on T-ZrO_2. The grey phase with a high intragranular porosity was enriched with europium and zirconium. The latter was assumed to be a solid solution based on $Eu_2Zr_2O_7$ (Py), as confirmed by the X-ray diffraction data (Table 1). Therefore, the number of T-phases increases with the ZrO_2 concentration.

The samples with 25 mol % ZrO_2-8.5 mol % CeO_2-66.5 mol % Eu_2O_3 and 30 mol % ZrO_2-8 mol % CeO_2-62 mol % Eu_2O_3 determine the boundaries of the two-phase region (Py+C). The microstructures of the samples characterizing the two-phase region (Py+C) are presented in Figures 4.5 j and g. Two types of grains were observed in the samples. Based on the qualitative micro-X-ray spectral analysis, it can be concluded that the dark phase enriched with zirconium contains less cerium and corresponds to a solid solution based on a pyrochlore-structured phase. The light phase corresponds to C-Eu_2O_3 because the amount of europium is slightly higher than that of the dark phase (Figure 5 h).

One of the characteristic features of the isothermal cross-section of the state diagram of the ZrO_2-CeO_2-Eu_2O_3 system at 1500 °C is the presence of three regions of solid solutions based on the cubic modification of ZrO_2 (CeO_2) with a fluorite-type structure. Just as a gap was observed in the ZrO_2-Eu_2O_3 double system, The field of the solid solutions based on the fluorite-type structure in the ternary system was broken in the region of formation of the ordered phase, which was similar to the gap in the solubility of the F-ZrO_2 phase in the region of the $Eu_2Zr_2O_7$ compound. The boundaries of the homogeneity regions of F-ZrO_2 extended from the corresponding coordinates of the ZrO_2-Eu_2O_3 limiting system (72-90 mol % ZrO_2 and 45-63 mol % ZrO_2). The concentration boundaries of the regions of homogeneity of the solid solutions based on F-ZrO_2 were curved toward the opposite side of the concentration triangle. The length of the F phase in the region with a high zirconium dioxide concentration was determined by samples with a cross-section of ZrO_2-(10 mol % CeO_2-90 mol % Eu_2O_3) and an iso-concentrate of 85 mol. % ZrO_2 containing 75 mol % ZrO_2-3 mol % CeO_2-22 mol % Eu_2O_3-two-phase (F-ZrO_2+Py), 80 mol % ZrO_2-2.5 mol % CeO_2-17.5 mol % Eu_2O_3 - single-phase (F-ZrO_2), 85 mol % ZrO_2-1.5 mol % CeO_2-13.5 mol % Eu_2O_3-biphasic (F-ZrO_2+T*). The maximum solubility of cerium dioxide in the solid solutions based on F-ZrO_2 was found to be 3 and 2 mol. %, respectively. The largest region of homogeneity was observed for the solid solution based on F-CeO_2. The boundary of the homogeneous region of the F-phase concaved towards the CeO_2 vertex and extended from the corresponding coordinates in the limiting ZrO_2-CeO_2 (56-100 mol % CeO_2) and CeO_2-Eu_2O_3 (80-100 mol % CeO_2) systems. The length of the F phase was determined by the two-phase samples with the composition of 17 mol % ZrO_2-75 mol % CeO_2-8 mol % Eu_2O_3 and 20 mol %

ZrO_2-75 mol % CeO_2-5 mol % Eu_2O_3 and single-phase sample with the composition of 13.5 mol % ZrO_2-80 mol % CeO_2-6.5 mol % Eu_2O_3. The parameters of the cubic unit cell with the fluorite structure vary from a = 0.5409 nm for pure CeO_2 to a = 0.5374 nm for the two-phase sample (F+C) of 17 mol % ZrO_2-75 mol % CeO_2-8 mol % Eu_2O_3 and up to a = 0.5319 nm for the three-phase sample (F+Py+C) of 37 mol % ZrO_2-45 mol % CeO_2-18 mol. % Eu_2O_3 (Figure 2, Table 1). The homogeneous regions in the cubic solid solutions with the fluorite-type structure were confirmed by the X-ray diffraction, petrographic and microstructural studies. The characteristic microstructure of the single-phase region <F-CeO_2> is presented in Figure 5 k. Polyhedral <F-CeO_2> grains of 2 to 25 μm were observed at the fracture of the sample with 3 mol % ZrO_2-95 mol % CeO_2-2 mol % Eu_2O_3 in the cross-section of CeO_2- (67 mol % ZrO_2-33 mol % Eu_2O_3) (Figure 5 k). The samples containing 60 mol % ZrO_2-20 mol % CeO_2-20 mol % Eu_2O_3, 65 mol % ZrO_2-10 mol % CeO_2-25 mol % Eu_2O_3, 55 mol % ZrO_2-31.5 mol % CeO_2-13.5 mol % Eu_2O_3 and 53.5 mol % ZrO_2-36.5 mol % CeO_2-10 mol % Eu_2O_3 revealed two structural components with distinct morphologies. According to the micro-X-ray spectral analysis, the grey smooth phase corresponded to <F-CeO_2>, and the grey porous phase with a perforated structure was identified as $Eu_2Zr_2O_7$. The electron microscopy results were confirmed by X-ray diffraction and petrography. The cross-section of ZrO_2-(50 mol % CeO_2-50 mol % Eu_2O_3) in the sample containing 60 mol % ZrO_2-20 mol % CeO_2-20 mol % Eu_2O_3 showed two isotropic phases F-CeO_2 and $Eu_2Zr_2O_7$ in equal amounts. In the sample containing 55 mol % ZrO_2-31.5 mol % CeO_2-13.5 mol % Eu_2O_3 in the cross-section of ZrO_2-(70 mol % CeO_2-30 mol % Eu_2O_3), there was an increase in the number of pyrochlore-type phases and a resultant change in the morphology of the samples.

The fluorite-structured phase was observed in the two-phase (C+F), (Py+F), (T+F) and three-phase (Py+F+T), (Py+C+F) regions.

The isothermal cross-section of the partial ZrO_2-$Eu_2Zr_2O_7$-CeO_2 system at 1500 °C was characterized by two three-phase (Py+F+T) and five two-phase (two Py+F, two T+F, one Py+T) regions.

The microstructures of the samples corresponding to the three-phase region (Py+F-ZrO_2+T-ZrO_2) by the cross-sections of ZrO_2-(50 mol % CeO_2-50 mol % Eu_2O_3) and ZrO_2-(30 mol % CeO_2-70 mol % Eu_2O_3) were characterized by the presence of morphologically different phases (Figure 5 o). Based on the scanning electron microscopy results of the sample containing 80 mol % ZrO_2-6 mol % CeO_2-14 mol % Eu_2O_3, a grey smooth phase corresponded to <F-ZrO_2>, and the grey porous phase with a perforated structure was typical of $Eu_2Zr_2O_7$ (Py). The matrix showed the inclusion of a dark grey phase <T-ZrO_2>.

The samples containing 65 mol % ZrO_2-25 mol % CeO_2-10 mol % Eu_2O_3, 70 mol % ZrO_2-21 mol % CeO_2-9 mol % Eu_2O_3, 75 mol % ZrO_2-16.5 mol % CeO_2-8.5 mol % Eu_2O_3, 80 mol % ZrO_2-14 mol % CeO_2-6 mol % Eu_2O_3, 85 mol % ZrO_2-9.5 mol % CeO_2-5.5 mol % Eu_2O_3 by cross-section ZrO_2-(70 mol % CeO_2-30 mol % Eu_2O_3), 57 mol % ZrO_2-38 mol % CeO_2-5 mol % Eu_2O_3 in cross-section Eu_2O_3-(60 mol % ZrO_2-40 mol % CeO_2) and 85 mol % ZrO_2-11 mol % CeO_2-4 mol % Eu_2O_3, 85 mol % ZrO_2-12 mol % CeO_2-3 mol % Eu_2O_3, 85 mol % ZrO_2-13 mol % CeO_2-2 mol % Eu_2O_3 along with the isoconcentrate 85 mol % ZrO_2 corresponded to the three-phase region (Py+F-CeO_2+T-ZrO_2). The structural components of the samples were different (Figure 5 p). From the results of the qualitative micro-X-ray spectral analysis, it was concluded that the light grey smooth phase corresponded to F-CeO_2, light grey porous with a perforated structure was associated with $Eu_2Zr_2O_7$, and the dark phase belonged to T-ZrO_2. The electron microscopy data were confirmed by the X-ray diffraction and petrography results. The cross-section of ZrO_2-(70 mol % CeO_2-30 mol % Eu_2O_3) in the sample with a composition

of 65 mol % ZrO_2-25 mol % CeO_2-10 mol % Eu_2O_3 displayed two isotropic phases F-ZrO_2 and Py in equal amounts and a small amount of anisotropic T-ZrO_2 phase with a high refractive index (n~2.06). According to the petrography results for the sample containing 70 mol % ZrO_2-21 mol. % CeO_2-9 mol % Eu_2O_3, there were two isotropic phases with inhomogeneous distributions. Thus, there was an increase in the number of isotropic phases. The sample containing 75 mol % ZrO_2-16.5 mol % CeO_2-8.5 mol % Eu_2O_3 showed a light porous isotropic phase (Py) constituting a smooth darker phase in the form of small inclusions of the isotropic nature (F-CeO_2) and intergranular inclusions of the anisotropic phase (T-ZrO_2). The isotropic phase (F-CeO_2) with numerous intergranular anisotropic inclusions (T-ZrO_2) exists as a matrix in the sample with 80 mol % ZrO_2-14 mol % CeO_2-6 mol % Eu_2O_3 along with significantly small amounts of another isotropic phase with a pyrochlore structure (Py). The structure becomes finer with the increase in the concentration of zirconium dioxide. The sample containing 85 mol % ZrO_2-9.5 mol % CeO_2-5.5 mol % Eu_2O_3 was based on the isotropic F-CeO_2 phase with isotropic inclusions of $Eu_2Zr_2O_7$. The boundaries of the three-phase region (Py+F-CeO_2+T-ZrO_2) determine the samples in the cross-section of Eu_2O_3-(60 mol % ZrO_2-40 mol % CeO_2) and along the 85 mol % ZrO_2 isoconcentrate. All the structural components possessed different textures and properties. The sample with 57 mol % ZrO_2-38 mol % CeO_2-5 mol % Eu_2O_3 displayed an isotropic phase (F) interspersed with an anisotropic phase (T) and a second isotropic phase (Py). In the sample containing 85 mol % ZrO_2-12 mol % CeO_2-3 mol % Eu_2O, the anisotropic dark phase <T-ZrO_2> acted as a matrix. Also, ZrO_2 grains were observed at the fracture along with the second isotropic light phase possessing the fluorite-structured <F-CeO_2> and separate intergranular isotropic inclusions of the light porous phase (Figure 4.5 n). The pyrochlore-structured phase was observed in small quantities within the samples. The number of Py phases gradually decreased with the increase in the cerium dioxide concentration. The two-phase sample with a composition of 85 mol % ZrO_2-14 mol % CeO_2-1 mol % Eu_2O_3 exhibited a dark anisotropic phase of partially stabilized <T-ZrO_2>, which formed the basis and constituted the second phase as small inclusions of isotropic <F-CeO_2> phase.

The isothermal cross-section of the partial system Eu_2O_3 $Eu_2Zr_2O_7$-CeO_2 at 1500 °C intersected two three-phase (C+Py+F-CeO_2, C+Py+F-ZrO_2) and six two-phase (C+B, C+F-CeO_2, C+F-ZrO_2, Py+F-ZrO_2, Py+C, Py+F-CeO_2) regions.

The subsystem with a low ZrO_2 concentration exhibited regions of solid solutions based on F-CeO_2, B-Eu_2O_3, C-Eu_2O_3, and F-ZrO_2 and pyrochlore-structured $Eu_2Zr_2O_7$ (Py) phases. The homogeneous region of the solid solution based on B-Eu_2O_3 extended from 1 mol % CeO_2 and 3 mol % ZrO_2 in the corresponding binary systems and passed through the sample containing 0.5 mol % ZrO_2-0.5 mol % CeO_2-99 mol % Eu_2O_3 in the cross-section of Eu_2O_3- (60 mol % ZrO_2-40 mol % CeO_2). The boundaries of the biphasic region (B+C) with a composition of 9.5 mol % ZrO_2-8.5 mol % CeO_2-85 mol % Eu_2O_3, 10 mol % ZrO_2-9.5 mol % CeO_2-80.5 mol % Eu_2O_3 were confirmed by the X-ray diffraction analysis of the samples of Eu_2O_3-(60 mol % ZrO_2-40 mol % CeO_2) and ZrO_2-(10 mol % CeO_2-90 mol % Eu_2O_3) (Table 1). The samples containing 2 mol % ZrO_2-10 mol % CeO_2-88 mol % Eu_2O_3, 3 mol % ZrO_2-10 mol % CeO_2-87 mol % Eu_2O_3, 4 mol % ZrO_2-9.5 mol % CeO_2-86.5 mol % Eu_2O_3, 5 mol % ZrO_2-9.5 mol % CeO_2-85.5 mol % Eu_2O_3 in the cross-section of ZrO_2-(10 mol % CeO_2-90 mol % Eu_2O_3) and 9.5 mol % ZrO_2-5.5 mol % CeO_2-85 mol % Eu_2O_3, 6 mol % ZrO_2-4 mol % CeO_2-90 mol % Eu_2O_3, 3 mol % ZrO_2-2 mol % CeO_2-95 mol % Eu_2O_3, 2.5 mol % ZrO_2-1.5 mol % CeO_2-96 mol % Eu_2O_3, 2 mol % ZrO_2-1 mol % CeO_2-97 mol % Eu_2O_3, 1.5 mol % ZrO_2-0.5 mol % CeO_2-98 mol % Eu_2O_3, and 0.5 mol % ZrO_2-0.5 mol % CeO_2-99 mol % Eu_2O_3 in the cross-section of Eu_2O_3- (60 mol % ZrO_2-40 mol % CeO_2) (Figure 5 q) displayed two-phase microstructures. Both the phases were uniformly

distributed in texture and contrast. According to the results of the qualitative X-ray spectral analysis, the grey phase corresponded to <C-Eu_2O_3>, and the light phase corresponded to <B-Eu_2O_3>.

The boundary of the homogeneous region of the C-modification of Eu_2O_3 was curved towards the side of the concentration triangle of the limiting binary system ZrO_2-CeO_2 to the vertex of CeO_2 and extended from the corresponding coordinates in the limiting CeO_2-Eu_2O_3 (18-25 mol % CeO_2) and ZrO_2-Eu_2O_3 mol % ZrO_2) system. The length of the C-phase was determined from the single-phase samples with the compositions of 15 mol % ZrO_2-9 mol % CeO_2-76 mol % Eu_2O_3 in the cross-section ZrO_2-(10 mol % CeO_2-90 mol % Eu_2O_3), 5 mol % ZrO_2-29 mol % CeO_2-66 mol % Eu_2O_3, and 10 mol % ZrO_2-27 mol % CeO_2-63 mol % Eu_2O_3 in the cross-section of ZrO_2-(30 mol % CeO_2-70 mol % Eu_2O_3). The radiographic data were consistent with the results of the microstructural and petrographic studies. The concentration dependencies of the C-phase unit cell parameters are presented in Figures 2-4.

The XRD patterns of the ZrO_2-CeO_2-Eu_2O_3 system at 1500 °C are presented in Figure 6.

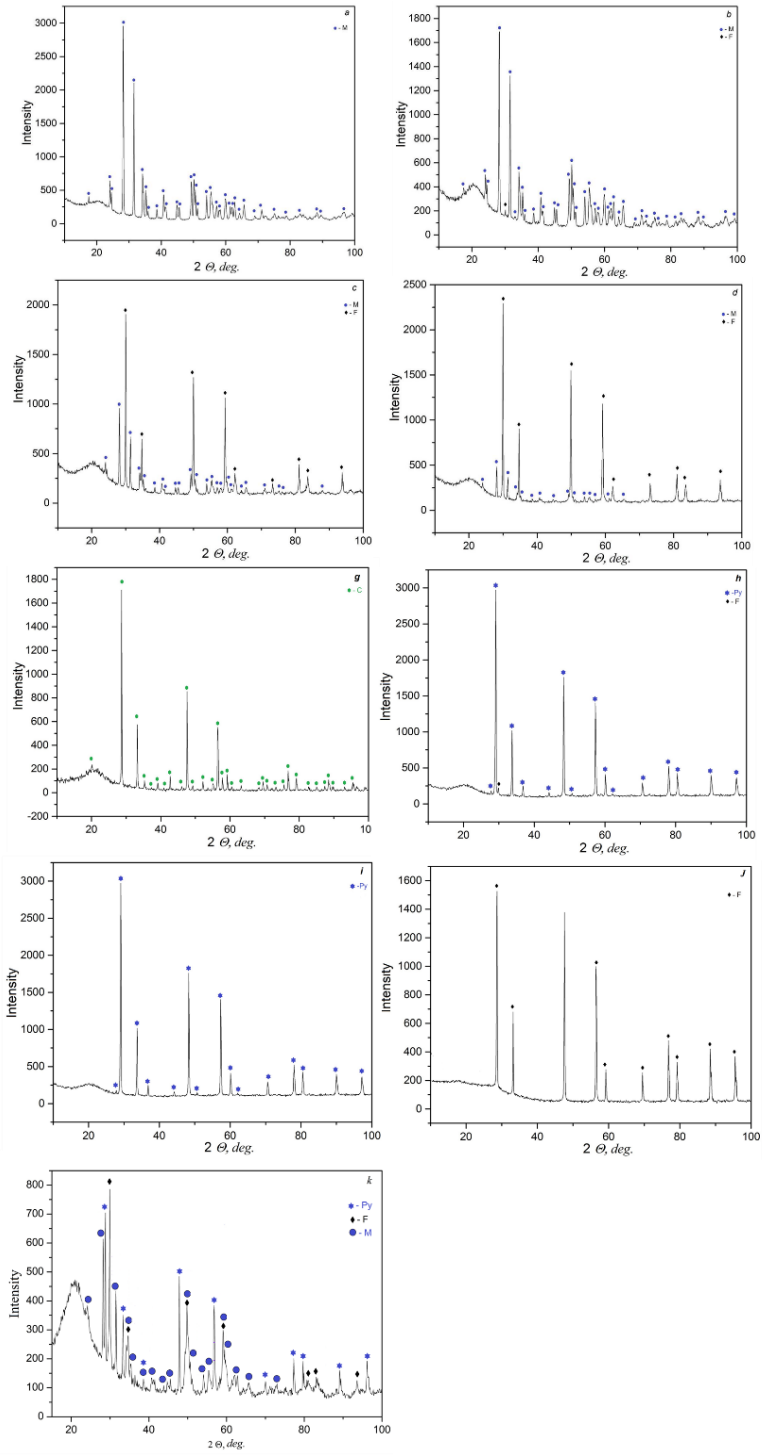

Figure 6 XRD patterns of the ZrO_2-CeO_2-Eu_2O_3 samples annealed at 1500 °C: **a-**90 mol % La_2O_3—10 mol % Sm_2O_3, (<A> *); **b**-40 mol % La_2O_3—60 mol % Sm_2O_3, (<A> * + <B>);**c-** 15 mol % La_2O_3—85 mol % Sm_2O_3, (<B>).The isothermal cross section of the ZrO_2-CeO_2-Eu_2O_3 system at 1500 °C constitutes seven single-phase (one B-Eu_2O_3, C-Eu_2O_3, F-CeO_2, Py, T-ZrO_2, two F-ZrO_2) ten two-phase-Eu_2O_3, C-Eu_2O_3+F-CeO_2, C-Eu_2O_3+F-ZrO_2, two Py+F-ZrO_2, F-ZrO_2+T-ZrO_2, Py+T-ZrO_2, Py+C-Eu_2O_3, Py+F-CeO_2, T-ZrO_2+F-CeO_2) and four three-phase (C-Eu_2O_3+F-CeO_2+Py, C-Eu_2O_3+F-ZrO_2+Py, Py+F-ZrO_2 +T-ZrO_2, Py+F-CeO_2+T-ZrO_2) regions.

4. Conclusions

The phase equilibria of the ternary ZrO_2-CeO_2-Eu_2O_3 system were studied for the first time, and the isothermal cross-section at a temperature of 1500 °C was constructed. The solid solutions were formed on the basis of the tetragonal (T) and cubic (F) phases with a fluorite-structured modification of ZrO_2, monoclinic (B) and cubic (C) modifications of Eu_2O_3, cubic modification with fluorite (F)-structured CeO_2 and an ordered pyrochlore-structured $Eu_2Zr_2O_7$ (Py) phase.

Author Contributions

Synthesis of powders for studding of state diagram based ZrO_2, CeO_2, Eu_2O_3 (**Y.M. Bataev, S.V. Yushkevych**). The samples for the microstructural studied using the scanning electron microscope SUPERPROBE-733 (**A.V. Sameljuk**). The X-ray diffraction (XRD) pattern (**O.A. Kornienko**). The manuscript preparation (**O.R. Andrievskaya, O.A. Kornienko**).

Competing Interests

The authors have declared that no competing interests exist.

References

1. Motoc AM, Valsan S, Slobozeanu AE, Corban M, Valerini D, Prakasam M, et al. Design, fabrication, and characterization of new materials based on zirconia doped with mixed rare earth oxides: Review and first experimental results. Metals. 2020; 10: 1-23.
2. Haladzhun Z, Trishchuk O, Figol N, Volyk N, Bandazheuski Y, Dubovaya N, et al. Innovative scientific researches: European development trends and regional aspect. 4th ed. Riga, Latvia: Baltija Publishing; 2020.
3. Zhang J, Guo XY, Jung YG, Li L, Knapp J. Lanthanum zirconate based thermal barrier coatings: A review. Surf Coat Technol. 2016; 323: 18-29.
4. Guo XY, Lu Z, Jung YG, Zhang J. Novel lanthanum zirconate-based thermal barrier coatings for energy applications. Switzerland: Springer, Cham; 2021.
5. Kilner JA, Burriel M. Materials for intermediate-temperature solid-oxide fuel cells. Annu Rev Mater Res. 2014; 44: 365-393.
6. Frolov AA, Andrievskaya ER, Kornienko OA, Frolov YA. Specifics of crystallization of highly refractory alloys based on zirconium, yttrium, and erbium oxides. Refrac Ind Ceram. 2007; 48: 185-188.
7. Wang BY, Zhu B, Yun SN, Zhang W, Xia C, Afzal M, et al. Fast ionic conduction in semiconductor $CeO_{2-\delta}$ electrolyte fuel cells. NPG Asia Mater. 2019; 11: 1-12.
8. Malutin AV, Lieberman EY, Mikhailichenko AI, Avetisov IH, Koshkin AG, Konkova TV. Catalytic activity of nanodispersed solid solutions $M_{0,1}Zr_{0,18}Ce_{0,72}O_2$, where M is a rare earth metal, in the oxidation reaction of carbon dioxide. Catal Ind. 2013: 54-59. Available from: https://istina.msu.ru/publications/article/73489248/.
9. Abe H. Current Status and Future of the Car Exhaust Catalyst Should Aim For ~ Tsukuba Innovation Arena (TIA): Outline and Outlook ~. Available from: https://ci.nii.ac.jp/naid/120006590728/.

10. Tyrsted C, Becker J, Hald P, Bremholm M, Pedersen JS, Chevallier J, et al. In-situ synchrotron radiation study of formation and growth of crystalline $Ce_xZr_{1-x}O_2$ nanoparticles synthesized in supercritical water. Chem Mater. 2010; 22: 1814-1820.
11. Bugrov AN, Rodionov IA, Zvereva IA, Smyslov RY, Almjasheva OV. Photocatalytic activity and uminescent properties of Y, Eu, Tb, Sm and Er-doped ZrO_2 nanoparticles obtained by hydrothermal method. Int J Nanotechnol. 2016; 13: 147-157.
12. Kim JR, Lee KY, Suh MJ, Ihm SK. Ceria-zirconia mixed oxide prepared by continuous hydrothermal synthesis in supercritical water as catalyst support. Catal Today. 2012; 185: 25-34.
13. Longo V, Roitti S. Solid state phase relations in the system CeO_2-ZrO_2. Ceramurgia Int. 1971; 1: 4-10.
14. Tani E, Yoshimura M, Somiya S. Revised phase diagram of the system ZrO_2-CeO_2 bellow 1400 °C. J Am Ceram Soc. 1983; 66: 506-510.
15. Duran P, Gonzales M, Moure C, Jurado JR, Pascual C. A new tentative phase equilibrium diagram for the ZrO_2-CeO_2 system in air. J Mater Sci. 1990; 25: 5001-5006.
16. Andrievskaya ER, Lopato LM. Interaction of cerium oxide with hafnium, zirconium, and yttrium oxides at 1500°C. Powder Powder Metall Met Ceram. 2001; 40: 405-413.
17. Panova TI, Glushkova VB, Nefedova MY. Investigation into the phase formation in the ZrO_2-CeO_2 system. Glass Phys Chem. 2005; 31: 240-245.
18. Andrievskaya ER, Gerasimyuk GI, Kornienko OA, Samelyuk AV, Lopato LM, Red'ko VP. Phase equilibria in the system HfO_2-ZrO_2-CeO_2 at 1500°C. Powd Metall Met Ceram. 2006; 45: 448-456.
19. Rouanet A. Contribution a l'etude des systemes zirconia - oxydes des lanthanides au voisinage de la fusion: Memoire de these. Rev Intern Hautes Temp Refract. 1971; 8: 161-180.
20. Andrievskaya ER, Gerasimyuk GI, Kornienko OA, Samelyuk AV, Lopato LM. Phase equilibria in the HfO_2-ZrO_2-CeO_2 system at 1250 deg C. Neorg Mater. 2006; 42: 1481-1488.
21. Andrievskaya ER, Lopato LM. Influence of composition on the T⇆M transformation in the systems ZrO_2-Ln_2O_3 (Ln = La, Nd, Sm, Eu). J Mater Sci. 1995; 30: 2591-2596.
22. Lopato LM, Andrievskaya ER, Shevchenko AV, Red`ko VP. Phase ratios in ZrO_2-Eu_2O_3 system. Zhurnal Neorganicheskoj Khimii. 1997; 42: 1736-1739.
23. Kornienko O, Bykov O, Sameliuk A, Yurchenko Y. Phase relation studies in the CeO_2-La_2O_3-Eu_2O_3 system at 1250 °C. Ukr Chemistr J. 2020; 86: 35-47.
24. Toropov SA. Phase diagrams of the refractory oxide systems, binary systems, chapter 3. Leningrad, Nauka. 1987; 5: 264.
25. Kuto T. Oxygen Ion conduction of fluorite-Type $Ce_{1-x}Ln_xO_{2-x/2}$ (Ln= lanthanide Element). J Electrochem Soc. 1975: 142-147.
26. Andrievskaya OR, Kornienko OA, Bykov OI, Chudinovich OV, Spasonova LN. The interaction between cerium dioxide, lanthanum and europium oxides at 1500 °C. Proc Appl Ceram. 2021; 15: 32-39.
27. Andrievskaya ER, Kornienko OA, Sameliuk AV, Sair A. Phase relation studies in the CeO_2-Eu_2O_3 system at 1500 to 600 °C in air. J Eur Ceram Soc. 2020; 40: 751-758.
28. Minervini L, Grimes RW, Sickafus KE. Disorder in pyrochlore oxides. J Am Ceram Soc. 2000; 83: 1873-1878.

29. Blanchard PE, Liu S, Kennedy BJ, Ling CD, Avdeev M, Aitken JB, et al. Investigating the local structure of lanthanoidhafnates Ln_2Hf_2O7 via diffraction and spectroscopy. J Phys Chem C. 2003; 117: 2266-2273.
30. Subramanian MA, Aravamudan G, Subba Rao GV. Oxide pyrochlores - a review. Prog Solid State Chem. 1983; 15: 55-143.
31. Andrievskaya ER. Phase equilibria in the systems of hafnia, yttria with rare-earth oxides. Scientific book Project, Kiev, Naukova Dumka. 2010. p.470.
32. Andrievskaya ER. Phase equilibria in the refractory oxide systems of zirconia, hafnia and yttria with rare-earth oxides. J Eur Ceram Soc. 2008; 28: 2363-2388.
33. Hinatsu Y, Muromura T. Phase relations in the systems ZrO_2-Y_2O_3-Nd_2O_3 and ZrO_2-Y_2O_3-CeO_2. Mater Res Bull. 1986; 21: 1343-1349.
34. Andrievskaya ER, Kornienko OA, Sayir A, Vasylkiv OO, Sakka Y. Phaserelation studies in the ZrO_2-CeO_2-La_2O_3system at 1500 °C. J Am Ceram Soc. 2011; 94: 1911-1919.
35. Haladzhun Z. Phase equilibria in the systems with ZrO_2, CeO_2 and Dy_2O_3. In: Innovative scientific researches: European development trends and regional aspect. 4th ed. Riga, Latvia: Baltija Publishing; 2020.
36. Grover V, Tyagi AK. Phase relation studies in the CeO_2-Gd_2O_3-ZrO_2 system. J Solid State Chem. 2004; 177: 4197-4204.
37. Korniienko OA, Bykov AI, Andrievskaya ER, Makudera AA. Phase equilibria in the ZrO_2-CeO_2-Yb_2O_3 system at 1100°C. Powder Metall Met Ceram. 2020; 59: 342-349
38. Kornienko OA, Andrievskay OR, Barshchevskaya HK. Phase relations in the system ternary based on ceria, zirconia and ytterbia at 1500 °C. J Chem Technol. 2020; 28: 142-152.